PHYSICAL REVIEW A **73**, 033410 (2006)

Time-dependent theoretical description of molecular autoionization produced by femtosecond xuv laser pulses

José Luis Sanz-Vicario,[1,2] Henri Bachau,[3] and Fernando Martín[1]
[1]*Departamento de Química, C-9, Universidad Autónoma de Madrid, 28049 Madrid, Spain*
[2]*Servicio de Investigación Universitaria (SIU), Instituto de Física, Universidad de Antioquia, Medellín, Colombia*
[3]*Centre des Lasers Intenses et Applications (UMR 5107 du CNRS-CEA—Université de Bordeaux I), 351 Cours de la Libération, F-33405 Talence, France*

(Received 5 December 2005; published 8 March 2006)

We present a nonperturbative time-dependent theoretical method to study H_2 ionization with femtosecond laser pulses when the photon energy is large enough to populate the Q_1 (25–28 eV) and Q_2 (30–37 eV) doubly excited autoionizing states. We have investigated the role of these states in dissociative ionization of H_2 and analyzed, in the time domain, the onset of the resonant peaks appearing in the proton kinetic energy distribution. Their dependence on photon frequency and pulse duration is also analyzed. The results are compared with available experimental data and with previous theoretical results obtained within a stationary perturbative approach. The method allows us as well to obtain dissociation yields corresponding to the decay of doubly excited states into two H atoms. The calculated H(n=2) yields are in good agreement with the experimental ones.

DOI: 10.1103/PhysRevA.73.033410 PACS number(s): 33.80.Rv, 33.80.Eh

I. INTRODUCTION

Recent developments in xuv laser technology have made possible generation and manipulation of laser pulses with femto-(fs) and subfemtosecond (sub-fs) durations and tunable intensities between 10^{10} and 10^{15} W/cm^2 [1–7]. This experimental progress has led to new developments on the theoretical side to deal with nonlinear processes resulting from the interaction of atoms and molecules with intense laser fields (see, for instance, Ref. [8] and references therein). The interest in using xuv fs sub-fs pulses is twofold. First, xuv radiation is ideal to efficiently ionize simple atoms [6,7,9,10] and molecules through absorption of a small number of photons. Second, pulses of such short duration allow one to investigate ionization at the atomic and molecular time scales. Thus, e.g., recent experiments on rare gas atoms using ultrashort xuv pulses have been able to show the exponential time decay of autoionizing states [11]. Such a decay typically occurs in the fs time scale. In molecules, the decay of autoionizing states is more complicated due to the presence of the nuclear motion. Vibration, dissociation, and rotation typically occur in the fs time scale and, therefore, may compete efficiently with autoionization [12,13]. Therefore, using xuv fs pulses can be very helpful to elucidate the competing mechanisms and to provide a temporal picture of autoionization that is necessarily different from that in atoms.

For the simplest H_2 molecule, doubly excited autoionizing states can be formed by absorption of photons with energy larger than 23 eV (see Fig. 1). These states lie above the $^2\Sigma_g^+$ ($1s\sigma_g$) ionization threshold and are repulsive. Thus they may either (i) autoionize yielding $H_2^+ + e^-$ (nondissociative ionization) and $H^+ + H + e^-$ (dissociative ionization) or (ii) dissociate yielding $H(nl) + H(n'l')$ and $H^+ + H^-$. In case (i), the ejected electron absorbs part of the total energy, leaving the H_2^+ ion in an excited vibrational state. When this vibrational state lies above the dissociation threshold, the residual H_2^+ ion dissociates into $H + H^+$. The latter process only contributes a few percent to the total photoionization cross section. In case (ii), the doubly excited states do not autoionize (because the autoionization lifetime is very large) and the system follows the corresponding repulsive potential energy curve until it dissociates into either two hydrogen atoms or a proton and H^-.

The clearest experimental evidence of H_2 autoionizing states has been obtained by analyzing the proton kinetic energy distribution (KED) arising from the dissociative ionization process [14–17]. The KED exhibits pronounced peaks that have been associated with several doubly excited states of $^1\Sigma_u^+$ or $^1\Pi_u$ symmetries. The origin of these peaks has been interpreted theoretically in the framework of a perturbative stationary approach [12,13,18]. The theory has also shown that several additional structures observed in the measured KED are due to interferences between direct photoionization and dissociative autoionization, which prevents one from interpreting the experimental results in terms of simple classical or semiclassical pictures. In contrast with the richness of the KED spectra, the H_2 photoelectron spectrum barely shows any trace of autoionizing states [19]. This is because the vibrational motion in the dominant $H_2^+ + e^-$ channel washes out the resonant peaks (however, they would become apparent if the final H_2^+ vibrational distribution were measured).

A straightforward (but computationally involved) approach for studying the interaction of a molecule with a time-dependent laser pulse is to solve the time-dependent Schrödinger equation. In this work, we propose a practical method to solve this equation by using an L^2-integrable Feshbach formalism which makes use of B-spline basis functions to represent both the electronic and the nuclear wave functions. The method is specially designed to describe molecular autoionization and takes into account all electronic

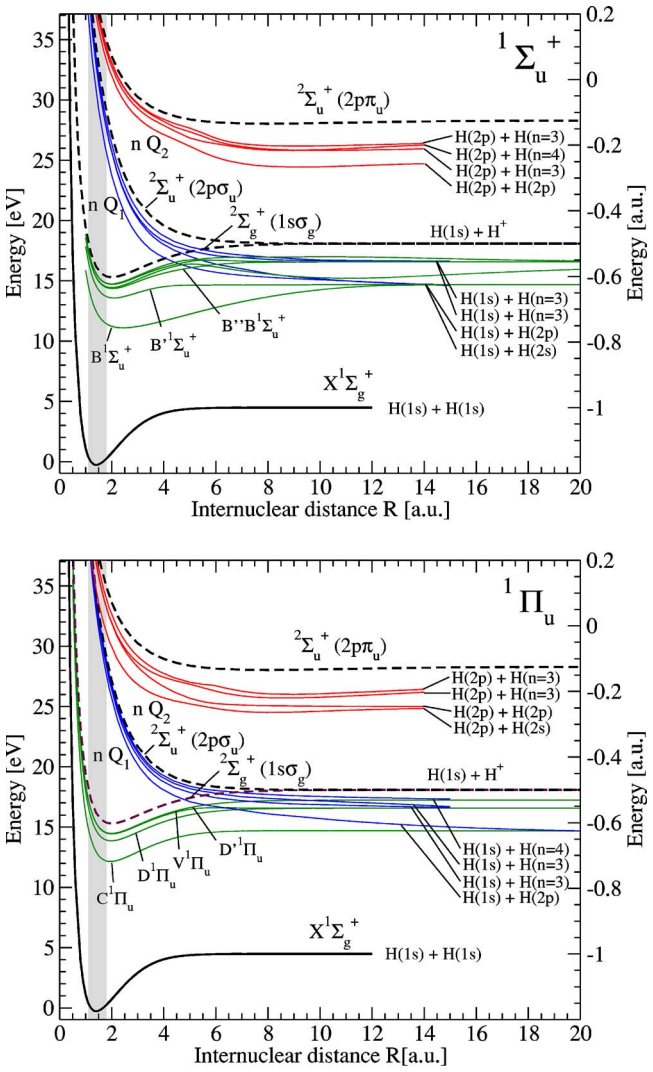

FIG. 1. (Color online) Potential energy curves of Q_1 and Q_2 $^1\Sigma_u^+$ and $^1\Pi_u$ autoionizing states of H_2. The ground state $X\,^1\Sigma_g^+$ (black solid line) and intermediate bound excited states of H_2 (green) and the ground $^2\Sigma_g^+$ and excited $^2\Sigma_u^+$, $^2\Pi_u$ states of H_2^+ are also shown (dashed lines). The H(nl)+H($n'l'$) dissociation limits for the first four resonances Q_1 (blue) and Q_2 (red) in each symmetry are indicated. The shaded vertical band represents the Franck-Condon region.

and vibrational degrees of freedom. Therefore, it allows one to describe the interplay between electronic and nuclear motions, and to visualize in the time domain the competition between the various processes in which doubly excited states are involved. Previous solutions of the time-dependent Schrödinger equation that include all electronic and vibrational degrees of freedom have been reported for the H_2^+ molecular ion [20–22] and the H_2 molecule [23]. In the latter work, the possibility of autoionization was not considered. The method proposed in this paper is thus an extension of the work of Ref. [23] to the region where doubly excited states play an important role.

The paper is organized as follows. In Sec. II we describe in detail the implementation of the time-dependent Schrödinger equation in the framework of the Feshbach approach. All the technical aspects of the calculations concerning the use of B-spline basis sets are given in Sec. III. In Sec. IV, we illustrate the performance of our method by comparing with KED spectra obtained within a perturbative stationary method [13,18] for photon energies between 25 and 28 eV (the region of the Q_1 doubly excited states; Sec. IV A) and between 30 and 37 eV (the region of the Q_2 doubly excited states; Sec. IV B). An additional complication in the latter case is the opening of ionization channels that can leave the residual H_2^+ ion in an excited dissociative state. Another potential application of the method is the evaluation of cross sections for dissociation into H+H (i.e., when there is no autoionization). Results for this process are presented in Sec. IV C. We end the paper with some conclusions and perspectives in Sec. V. Atomic units are used throughout unless otherwise stated.

II. THEORY

We solve the time-dependent Schrödinger equation (TDSE)

$$\left(\mathcal{H}(\mathbf{r},R,t) - i\frac{\partial}{\partial t}\right)\Phi(\mathbf{r},R,t) = 0 \tag{1}$$

where $\mathcal{H}$ is the total Hamitonian that includes the H_2 field-free Hamiltonian and the time-dependent perturbation potential $V(t)$,

$$\mathcal{H}(\mathbf{r},R,t) = \mathcal{H}^0(\mathbf{r},R) + V(t). \tag{2}$$

$V(t)$ represents the laser-molecule interaction potential in the dipole approximation, expressed in velocity or length gauge. In the velocity gauge it has the form $\mathbf{p}\cdot\mathbf{A}(t)$, where $\mathbf{p}$ is the dipole operator and $\mathbf{A}(t)$ is the vector potential. This vector potential corresponds to a pulse of duration T and photon energy ω, and is linearly polarized along the direction of the internuclear axis ($^1\Sigma_u^+$ final symmetry) or perpendicular to it ($^1\Pi_u$ final symmetry). Its module is defined in the time interval $[0,T]$ as

$$A(t) = A_0 \sin^2\left(\frac{\pi}{T}t\right)\cos(\omega t) \tag{3}$$

where A_0 is the potential amplitude, which is related to the laser peak intensity $A_0/\omega = [I\ (\mathrm{W/cm^2})/3.5095\times 10^{16}]^{1/2}$. The H_2 Hamiltonian, neglecting mass polarization and relativistic correction terms, is written as

$$\mathcal{H}^0(\mathbf{r},R) = T(R) + \mathcal{H}_{el}(\mathbf{r},R) \tag{4}$$

where $T(R) = -\nabla_R^2/2\mu$ is the relative kinetic energy of the nuclei, μ is the reduced mass, and $\mathcal{H}_{el}$ is the electronic Hamiltonian (which includes the $1/R$ repulsion term). The vector $\mathbf{r}$ labels the set of electron coordinates and R corresponds to the internuclear distance.

Following the usual Feshbach procedure in which the nonresonant and resonant parts of the wave function are assigned to two orthogonal complementary subspaces $\mathcal{P}$ and $\mathcal{Q}=1-\mathcal{P}$, respectively, we will project the TDSE in the basis of molecular eigenstates associated with each subspace. As-

suming that nonadiabatic couplings are negligible [Born-Oppenheimer (BO) approximation], the eigenstates associated with the $\mathcal{P}$ subspace can be written as $\{\psi_{\alpha l\epsilon}(\mathbf{r},R)\chi_{v_\alpha}(R)\}$, where the electronic wave function $\psi_{\alpha l\epsilon}$ satisfies the projected equation for the nonresonant electron scattering

$$[\mathcal{P}\mathcal{H}_{el}\mathcal{P}-\mathcal{E}(R)]\psi_{\alpha l\epsilon}(\mathbf{r},R)=0, \quad \mathcal{E}(R)=E_\alpha(R)+\epsilon, \quad (5)$$

where α denotes the full set of quantum numbers for the electronic state of the residual molecular ion H_2^+ with BO energy $E_\alpha(R)$ at the internuclear distance R. The indices l and ϵ denote, respectively, the angular momentum and the kinetic energy of the ejected electron. The nuclear wave function χ_{v_α} satisfies the equation

$$[T(R)+\mathcal{E}(R)-W_{v_\alpha}]\chi_{v_\alpha}(R)=0 \quad (6)$$

where W_{v_α} is the vibronic energy (electronic plus vibrational) in channel α. The eigenstates associated with the $\mathcal{Q}$ subspace are written as $\{\phi_r(\mathbf{r},R)\Upsilon_{k_r}(R)\}$, where ϕ_r is the electronic wave function of the r autoionizing state that satisfies the projected Schrödinger equation

$$[\mathcal{Q}\mathcal{H}_{el}\mathcal{Q}-\mathcal{E}_r(R)]\phi_r(\mathbf{r},R)=0 \quad (7)$$

where $\mathcal{E}_r(R)$ denotes the BO energy of the resonance r at the internuclear distance R, and the nuclear wave function Υ_{k_r} satisfies

$$[T(R)+\mathcal{E}_r(R)-W_{k_r}]\Upsilon_{k_r}(R)=0 \quad (8)$$

in which W_{k_r} corresponds to the vibronic energy of the resonant state r. The initial ground state of H_2 is written as $\{\psi_g(\mathbf{r},R)\chi_{v_g}(R)\}$, where ψ_g is an eigenstate of the unprojected $\mathcal{H}_{el}$ Hamiltonian and χ_{v_g} is the corresponding BO vibrational wave function. The corresponding vibronic energy is W_{v_g}.

We use the following expansion for the time-dependent wave function:

$$\begin{aligned}|\Phi(\mathbf{r},R,t)\rangle = {} & C_{gv_g}(t)\phi_g(\mathbf{r},R)\chi_{v_g}(R)e^{-iW_{v_g}t} \\ & + \sum_\alpha \sum_l \int d\epsilon \sum\!\!\!\!\!\!\int_{v_\alpha} C^l_{\alpha\epsilon v_\alpha}(t)\psi_{\alpha l\epsilon}(\mathbf{r},R)\chi_{v_\alpha}(R)e^{-iW_{v_\alpha}t} \\ & + \sum_r \sum\!\!\!\!\!\!\int_{k_r} C_{rk_r}(t)\phi_r(\mathbf{r},R)\Upsilon_{k_r}(R)e^{-iW_{k_r}t}. \end{aligned} \quad (9)$$

Introducing this ansatz into the TDSE, a system of coupled differential equations is obtained. By construction, the $\mathcal{P}$ and $\mathcal{Q}$ states are orthogonal. The ground state is not strictly orthogonal to the $\mathcal{P}$ and $\mathcal{Q}$ states with the same symmetry; however, since it is very similar to the lowest $\mathcal{P}$ state, orthogonality is approximately fulfilled if one excludes the latter $\mathcal{P}$ state from the expansion. Nevertheless, since in the present study we restrict ourselves to one-photon absorption, the $g \leftrightarrow u$ selection rule guarantees that for all effective transitions orthogonality is exactly fulfilled. Thus, for simplicity in the notation, we will assume that all states in expansion (9) are exactly orthogonal. Since $\mathcal{Q}$ and $\mathcal{P}$ states are eigenstates of different Hamiltonians ($\mathcal{Q}\mathcal{H}_{el}\mathcal{Q}$ and $\mathcal{P}\mathcal{H}_{el}\mathcal{P}$, respectively), they will be coupled by the exact $\mathcal{H}_{el}$ Hamiltonian, leading to the so-called electrostatic couplings. These $\mathcal{P}$-$\mathcal{Q}$ couplings will be responsible for autoionization of the ϕ_r doubly excited states to the nonresonant continuum states $\psi_{\alpha l\epsilon}$. Neglecting the small electrostatic couplings with the ground state, the set of coupled differential equations may be written in compact form in the interaction picture as

$$\begin{pmatrix} \dot{C}_{\mathrm{I},gv_g} \\ \dot{\mathbf{C}}_{\mathrm{I},rk_r} \\ \dot{\mathbf{C}}^l_{\mathrm{I},\alpha\epsilon v_\alpha} \end{pmatrix} = \begin{pmatrix} 0 & A(t)\mathbf{p}_{gv_g,rk_r} & A(t)\mathbf{p}^l_{gv_g,\alpha\epsilon v_\alpha} \\ A(t)\mathbf{p}_{rk_r,gv_g} & 0 & \mathcal{Q}\mathcal{H}\mathcal{P}^l_{rk_r,\alpha\epsilon v_\alpha} \\ A(t)\mathbf{p}^l_{\alpha\epsilon v_\alpha,gv_g} & \mathcal{P}H\mathcal{Q}^l_{\alpha\epsilon v_\alpha,rk_r} & 0 \end{pmatrix} \times \begin{pmatrix} C_{\mathrm{I},gv_g} \\ \mathbf{C}_{\mathrm{I},rk_r} \\ \mathbf{C}^l_{\mathrm{I},\alpha\epsilon v_\alpha} \end{pmatrix}. \quad (10)$$

Here the $\mathbf{C}_{\mathrm{I},rk_r}$ and $\mathbf{C}^l_{\mathrm{I},\alpha\epsilon v_\alpha}$ coefficients (written in the interaction picture) are associated with the vibronic states of the doubly excited state and the electronic continuum states, respectively. For the ground initial state $X\,^1\Sigma_g^+$, only the first vibrational state $v_g=0$ is included. The set of coupled differential equations given in Eq. (10) has been integrated up to a sufficiently large time ($t_{max}>T$) using the initial condition $C_{\mathrm{I},gv_g=0}(t=0)=1$.

At variance with the perturbative stationary method developed previously in Ref. [13], where the total scattering wave function is solved through the Lippman-Schwinger equation, in the present spectral method the total final-state wave function is built up by the time-dependent close-coupling propagation itself, a procedure that allows for the mixing of the $\mathcal{P}$ and $\mathcal{Q}$ spaces, through the $\mathcal{Q}\mathcal{H}_{el}\mathcal{P}$ electrostatic couplings. It is worth noting that, in this time-dependent procedure, the $\mathcal{Q}$ resonant states will be populated by the laser field only during the pulse duration, but can be depopulated by autoionization (i.e., through the $\mathcal{Q}\mathcal{H}_{el}\mathcal{P}$ couplings) at any time. All $\mathcal{Q}\mathcal{H}_{el}\mathcal{P}$ couplings vanish in the limit $t\to\infty$, except those associated with the Q_n ($n\geqslant 4$) doubly excited states that may also dissociate into doubly excited states of H^-. Since the latter states are barely populated by photon absorption [17], the condition $\mathcal{Q}\mathcal{H}_{el}\mathcal{P}\underset{t\to\infty}{\to}0$is always satisfied in practice. This means that, asymptotically, the electronic Hamiltonian is $\mathcal{Q}\mathcal{H}_{el}\mathcal{Q}+\mathcal{P}\mathcal{H}_{el}\mathcal{P}$. Thus, after time integration, the values of the expansion coefficients C_{gv_g}, $\mathbf{C}_{rk_r}$, and $\mathbf{C}^l_{\alpha\epsilon v_\alpha}$ in Eq. (9) directly provide the transition amplitudes to the different vibronic states. It is also worth stressing here that the Feshbach asymptotic condition for the $\mathcal{P}$ space, i.e., $\mathcal{P}\Phi\underset{t\to\infty}{\to}\Phi$, is automatically satisfied, which implies that transition amplitudes to $\mathcal{P}$ states have the meaning of ionization amplitudes. Nevertheless, since the $\mathcal{Q}\mathcal{H}_{el}\mathcal{P}$ couplings vanish asymptotically, the $\mathcal{Q}$ doubly excited states may still remain populated at $t=\infty$, which is the reason why dissociation into two neutral H atoms is also well described by the present formalism.

The ionization probability, differential in the W_{v_α} energy, is given by

$$\frac{dP}{dW_{v_\alpha}} = \sum_l \int d\epsilon |C^l_{\alpha\epsilon v_\alpha}(t=T)|^2. \quad (11)$$

For dissociative ionization, W_{v_α} is directly related to the center-of-mass energy of the outgoing protons, $E_{H^+} = W_{v_\alpha} - W_\infty$, where W_∞ is the energy of a H atom infinitely separated from H^+. For nondissociative ionization, W_{v_α} is the vibronic energy of the residual H_2^+ ion. Integrating Eq. (11) over W_{v_α} gives the total ionization probability P. The related cross section σ for N-photon absorption reads

$$\frac{d\sigma}{dW_{v_\alpha}}(\mathrm{cm}^{2N}\,\mathrm{s}^{N-1}/\mathrm{eV}) = \left(\frac{\omega}{I}\right)^N \frac{C'(N)}{T}\frac{dP}{dW_{v_\alpha}} \quad (12)$$

where I corresponds to the laser intensity in W cm^{-2}, T is the laser pulse duration in seconds, ω is the photon energy in joules, W_{v_α} is given in eV when it corresponds to the proton kinetic energy, and $C'(N)$ is a dimensionless coefficient taking into account the time dependence of the intensity. In our study, $N=1$ and $C'(1)=\frac{8}{3}$. For linearly polarized light and random orientation of the H_2 molecules, the cross section is the sum of the $^1\Sigma_u^+$ and twice the $^1\Pi_u$ components divided by 3. All calculations in this work have been performed for an intensity of 10^{12} W/cm^2. In this context, the definition of the cross sections is only justified for very long pulses, much longer than the autoionization lifetimes of the doubly excited states involved in the process. Nevertheless, for short pulses, we will still use cross sections as a practical way to renormalize and make direct comparisons between results obtained with different pulse durations.

III. CALCULATIONS

A. Electronic calculations

A standard configuration interaction (CI) procedure is used to obtain the ground state of H_2. Two kinds of orbitals are used in the CI expansion: H_2^+ and Slater-type orbitals. The H_2^+ orbitals are expanded in a basis of 140 B-splines of order $k=8$, built upon a linear knot sequence, with angular momentum up to $l=8$, and inside a radial box of size $r_{max}=60$ a.u. [24]:

$$\varphi_{nm} = \sum_{l=0}^{l_{max}} \sum_{i=0}^{N} c_i^{nl} \frac{B_i^k(r)}{r} \mathcal{Y}^{lm}(\hat{r}). \quad (13)$$

Slater-type orbitals (STOs), defined as $r^{n-1}\exp(-\gamma_{il}r)$, with $n=1-9$, angular momemtum $l=0-6$, and nonlinear parameters $\gamma_{il}=2.8$ for all i and l, are expanded in the same basis of B-spline functions. The STOs are placed in the middle of the molecular axis and are used to accelerate the convergence with respect to the number of two-electron configurations. The number of configurations used in the CI expansion is 400.

A restricted CI expansion, compatible with the use of the Feshbach approach, is used for the $\mathcal{Q}$ resonant states. Two-electron projection operators are built to satisfy the antisymmetry principle such that $\mathcal{P}(\mathbf{r}_1,\mathbf{r}_2)=\mathcal{P}(\mathbf{r}_1)+\mathcal{P}(\mathbf{r}_2)-\mathcal{P}(\mathbf{r}_1)\mathcal{P}(\mathbf{r}_2)$ and $\mathcal{Q}(\mathbf{r}_1,\mathbf{r}_2)=1-\mathcal{P}(\mathbf{r}_1,\mathbf{r}_2)$. To obtain the Q_1 doubly excited states, we use the one-electron projection operator $\mathcal{P}(\mathbf{r}_1)=|1s\sigma_g\rangle\langle 1s\sigma_g|$. The corresponding two-electron operator projects into configurations of the type $\Theta[1s\sigma_g(\mathbf{r}_1)\phi_{\epsilon l}(\mathbf{r}_2)]$ (i.e., one electron in the $1s\sigma_g$ orbital of the H_2^+ ion and the other elsewhere), where Θ is the symmetrization (antisymmetrization) operator for singlet (triplet) states. The operator $\mathcal{Q}$ projects into the complementary orthogonal subspace, which means that, in practice, the $1s\sigma_g$ must be removed from the basis of molecular orbitals used in the CI expansion of the Q_1 states. For the Q_2 states, $\mathcal{P}(\mathbf{r}_1)=|1s\sigma_g\rangle\langle 1s\sigma_g|+|2p\sigma_u\rangle\langle 2p\sigma_u|$, which projects into configurations of the type $\Theta[1s\sigma_g(\mathbf{r}_1)\phi_{\epsilon l}(\mathbf{r}_2)]$ and $\Theta[2p\sigma_u(\mathbf{r}_1)\phi_{\epsilon l}(\mathbf{r}_2)]$. This means that both $1s\sigma_g$ and $2p\sigma_u$ orbitals must be excluded from the CI expansion in the complementary $\mathcal{Q}$ subspace.

The Q_1 doubly excited states ϕ_r are obtained by diagonalizing the $\mathcal{Q}\mathcal{H}_{el}\mathcal{Q}$ Hamiltonian in the following configuration basis:

symmetry $^1\Sigma_u^+$: $1\sigma_u n\sigma_g$ $(n=2,70)$, $1\pi_u n\pi_g$ $(n=1,70)$, $2\sigma_g n\sigma_u$ $(n=2,35)$, $2\sigma_u n\sigma_g$ $(n=2,18)$, $3\sigma_g n\sigma_u$ $(n=1,18)$, $1\pi_g n\pi_u$ $(n=1,10)$, $1\delta_g n\delta_u$ $(n=1,10)$, and $2\pi_u n\pi_g$ $(n=1,10)$;

symmetry $^1\Pi_u$: $1\sigma_u n\pi_g$ $(n=1,70)$, $1\pi_u n\sigma_g$ $(n=2,70)$, $2\sigma_g n\pi_u$ $(n=2,35)$, $2\sigma_u n\pi_g$ $(n=1,18)$, $3\sigma_g n\pi_u$ $(n=2,18)$, $1\pi_g n\sigma_u$ $(n=3,10)$, $1\delta_g n\pi_u$ $(n=1,10)$, $2\pi_u n\sigma_g$ $(n=4,10)$, and $4\sigma_g n\pi_u$ $(n=2,10)$.

For the Q_2 doubly excited states, the configuration basis is

symmetry $^1\Sigma_u^+$: $1\pi_u n\pi_g$ $(n=1,70)$, $2\sigma_g n\sigma_u$ $(n=2,70)$, $2\sigma_u n\sigma_g$ $(n=3,18)$, $3\sigma_g n\sigma_u$ $(n=3,18)$, $1\pi_g n\pi_u$ $(n=2,10)$, $1\delta_g n\delta_u$ $(n=1,10)$, and $2\pi_u n\pi_g$ $(n=2,10)$;

symmetry $^1\Pi_u$: $1\pi_u n\sigma_g$ $(n=2,70)$, $2\sigma_g n\pi_u$ $(n=2,70)$, $2\sigma_u n\pi_g$ $(n=1,18)$, $3\sigma_g n\pi_u$ $(n=2,18)$, $1\pi_g n\sigma_u$ $(n=3,10)$, $1\delta_g n\pi_u$ $(n=1,10)$, $2\pi_u n\sigma_g$ $(n=4,10)$, and $4\sigma_g n\pi_u$ $(n=2,10)$.

The continuum wave functions $\psi_{\alpha l\epsilon}$ are computed using an $\mathcal{L}^2$ close-coupling approach. A set of orthogonal uncoupled continuum states (UCSs) are defined [25]:

$$\zeta_{\alpha l\epsilon}(\mathbf{r}_1,\mathbf{r}_2) = \Theta(\Psi_{\alpha l}(\mathbf{r}_1,\hat{r}_2)R_{\alpha l\epsilon}(r_2)) \quad (14)$$

where $R_{\alpha l\epsilon}$ is the radial wave function of the outgoing electron and $\Psi_{\alpha l}$ is the channel function, which corresponds to a state of H_2^+ combined with the angular part of the ejected electron to provide the correct channel symmetry. In practice, these UCSs are obtained by a separate diagonalization of the H_2 Hamiltonian in the bases of configurations $\Theta[1s\sigma_g(\mathbf{r}_1)\varphi_{klm}(\mathbf{r}_2)]$ and $\Theta[2p\sigma_u(\mathbf{r}_1)\varphi_{klm}(\mathbf{r}_2)]$, where φ_{klm} is obtained by diagonalizing the H_2^+ Hamiltonian for a fixed value of the angular momentum l. The configurations used to describe the UCSs are as follows:

symmetry $^1\Sigma_u^+$: $1\sigma_g n\sigma_u$ $(n=1,75)$ for $l=1$, 3, 5, and 7 and $1\sigma_u n\sigma_g$ $(n=1,75)$ for $l=2$, 4, 6 and 8;

symmetry $^1\Pi_u$: $1\sigma_g n\pi_u$ $(n=1,75)$ for $l=1$, 3, 5, and 7 and $1\sigma_u n\pi_g$ $(n=1,75)$ for $l=2$, 4, 6 and 8.

Diagonalization using these bases leads to discretized energy spectra $\{\varepsilon_{\alpha ln}\}$ and UCS wave functions $\tilde{\zeta}_{\alpha ln}$ normalized to the Kronecker δ. These UCSs are then renormalized to the Dirac δ function by using the density of states

$$\zeta_{\alpha l\varepsilon_n} = \rho^{1/2}_{\alpha ln}(\varepsilon_n)\tilde{\zeta}_{\alpha ln} \tag{15}$$

where $\rho_{\alpha ln}(\varepsilon_n)=2/(\varepsilon_{\alpha l(n+1)}-\varepsilon_{\alpha l(n-1)})$. Interchannel coupling between different l's is then introduced through the Lippman-Schwinger equation [25],

$$\psi_{\alpha l\varepsilon_n} = \zeta_{\alpha l\varepsilon_n} + \mathcal{G}^+(\varepsilon_n)V\zeta_{\alpha l\varepsilon_n} \tag{16}$$

where the Green's functions $\mathcal{G}^+$ have been evaluated from the system of linear equations that results from the projection of the above equation into the UCS basis [26]. In practice, the resulting coupled continuum electronic states $\psi_{\alpha l\varepsilon_n}$ are calculated in a chosen discretized energy grid $\{\varepsilon'_n\}$, equidistant in the vector $k=\sqrt{2\varepsilon'_n}$, since this choice simulates the spectrum that would be obtained from a box. We have also used an inverse interpolation procedure [25], by slightly varying the box size, to ensure that, for each angular momentum l, at least one of the UCS eigenvalues corresponds to a chosen grid energy ε'_n.

B. Vibrational wave functions

The vibrational wave functions are also expanded in terms of B-splines:

$$\chi_{v_\alpha}(R) = \sum_{i=1}^{N} c_i^{v_\alpha} B_i(R), \quad \Upsilon_{k_r}(R) = \sum_{i=1}^{N} c_i^{k_r} B_i(R). \tag{17}$$

We have used a basis set of 240 B-splines of order $k=8$ inside a box of $R_{max}=14$ a.u. for all vibrational wave functions. After diagonalizing Eq. (6), eigenvalues lying above the dissociation limit correspond to vibrational continuum states $\tilde{\chi}_{v_\alpha}$. Similarly, since Q_1 and Q_2 energy curves are repulsive, the diagonalization of Eq. (8) leads to $\tilde{\Upsilon}_{k_r}$ eigenfunctions, pertaining to the vibrational continuum as well. Both $\tilde{\chi}_{v_\alpha}$ and $\tilde{\Upsilon}_{k_r}$ wave functions are normalized to the Kronecker δ. To recover the proper Dirac δ normalization, the vibrational continuum states are also renormalized through the density of states:

$$\chi_{v_\alpha} = \rho^{1/2}_{v_\alpha}\tilde{\chi}_{v_\alpha}, \quad \Upsilon_{k_r} = \rho^{1/2}_{k_r}\tilde{\Upsilon}_{k_r}, \tag{18}$$

where ρ is the density of vibrational states given by $\rho_{v_\alpha}=2/(W_{v_\alpha+1}-W_{v_\alpha-1})$ and $\rho_{k_r}=2/(W_{k_r+1}-W_{k_r-1})$.

C. Time-dependent calculations

TDSE calculations require a careful choice of the box size, for both the electronic and the nuclear motion, to be compatible with the total laser pulse duration T. Since the pulse is built as a wave packet, the frequency spectra has a spectral width given by its Fourier transform,

$$\Delta\omega = \frac{2\pi}{T/2}. \tag{19}$$

In order to correctly treat the continuum spectra with a discretization method in the time propagation, the energy spacing between discretized states (both electronic and vibrational states) must be smaller than the spectral width. Thus the size of the electronic (nuclear) box has been chosen to comply with the restriction $\Delta\varepsilon_n \ll \Delta\omega$ ($\Delta W_{v_\alpha} \ll \Delta\omega$). By satisfying this condition, the electronic (nuclear) wave packet does not reach the limit of the electronic (nuclear) box before the end of the pulse, thus preventing unphysical reflections from the wall. Fulfilling the above conditions for the electronic wave packet is more difficult than for the nuclear wave packet due to the smaller mass of the electrons (the energy spacing in a box is inversely proportional to the square root of the mass). So, in practice, one starts with a predefined energy grid $\{\varepsilon'_n\}$ that does not satisfy the spectral width condition. Then, coupling matrix elements in a denser energy grid $\{\varepsilon''_n\}$ satisfying that condition are obtained by interpolation of the corresponding matrix elements and renormalizing with the correct density of states. This interpolation procedure allows us to choose the electronic grid at convenience for any given pulse duration. The typical pulse duration we use in this work is $T=10$ fs. Hence, the spectral width condition requires an electronic energy grid spacing of $\Delta\varepsilon<0.03$ a.u. In addition, to correctly describe autoionization of a ϕ_r doubly excited state at a given value of the internuclear distance, the electronic energy spacing must be smaller than the corresponding autoionization width Γ_r: $\Delta\varepsilon_n \ll \Gamma_r$. A typical value of the autoionization width for the lowest $Q_1\ ^1\Sigma_u^+$ doubly excited state in the Franck-Condon region is 0.03 a.u. [27]. Therefore, by choosing an energy grid that satisfies the spectral condition, the latter autoionization condition is automatically satisfied. In this work, the energy grid is constructed from an equidistant k grid. A suitable choice is $\Delta k=0.01-0.02$ a.u., which leads to a typical energy spacing $\Delta\varepsilon_n=0.008$ a.u. near the $Q_1\ ^1\Sigma_u^+$ states in the Franck-Condon region. The value of $\Delta\varepsilon_n$ becomes progressively smaller as the electronic energy approaches the ionization threshold. The vibrational energy spacing obtained from diagonalization of the vibrational equations is always lower than 0.03 a.u. for the box size used in this work (14 a.u.). Therefore, in this case, we have directly used the energy grid resulting from the diagonalization of the vibrational Hamiltonians.

In the perturbative limit of the TDSE, which is obtained for low laser intensities, the cross sections for inelastic processes are very small and the population of the ground initial state remains very close to unity. Therefore, one must be careful with the numerical procedure used to integrate the system of differential equations. We make use of a sixth-order Runge-Kutta method. We have checked that the norm of the total wave function is preserved to unity with deviations less than 10^{-5}. Integration has also been tested with a Bulirsch-Stoer integrator, providing results with similar precision.

In this work we have used a variety of pulse durations T. For all practical purposes, we have found that for pulses with $T\leqslant 10$ fs, a time integration limit $t_{max}=10$ fs leads to results identical to the long-time limit $t_{max}=\infty$.

IV. RESULTS AND DISCUSSION

A. Dissociative photoionization in the photon energy range $\omega=25-28$ eV

Our first goal is to assess the performance of the present time-dependent method by comparing its results with those

previously obtained by using stationary perturbation theory. Both methods should give similar results for low laser intensities and long pulses. In this work we have used a fixed laser intensity of $I=10^{12}$ W/cm^2. We shall concentrate mainly on the vibrational distributions: the H_2^+ vibrational distribution in nondissociative ionization, the proton KED in dissociative ionization, and the KED of neutral hydrogen atoms arising from (nonionizing) dissociation of doubly excited H_2.

Our first example is the final vibrational distribution for the final $^1\Sigma_u^+$ symmetry. This symmetry gives the contribution to the cross section of protons observed at 0° with respect to the polarization vector of the incident radiation. Both perturbative [13] and experimental results [16] are available in the photon energy range $\omega=25-28$ eV. It has been shown that the proton KED spectrum exhibits resonant peaks that are mainly due to the lowest Q_1 doubly excited state. This is in fact the only doubly excited state included in the early perturbative calculations of Ref. [12]. This was the first theoretical approach that included both the electronic and the vibrational degrees of freedom as well as possible interferences between all ionization and dissociation processes. For a meaningful comparison with the latter calculations, in the results presented in this section we have only included the Q_1 doubly excited state. In contrast with the $^1\Sigma_u^+$ symmetry, the $^1\Pi_u$ symmetry does not exhibit any resonant peak in this photon energy region and, therefore, will not be considered here.

Since the pulse duration T is finite, a band of final vibronic states will be populated from the ground state, which is at variance with perturbative calculations, in which the final state energy E is well defined. Nevertheless, in looking for a numerical solution of the TDSE, the number of vibronic states included in expansion (9) must be truncated. To achieve convergence with the number of vibronic states, our procedure is to define energy bands ΔE of increasing width centered on the energy $E=W_{gv_g}+\omega$. The band must include all vibronic states associated with the doubly excited state and with all electronic continuum states of the $\{\varepsilon_n''\}$ grid that are enclosed in the selected energy region. As we will see below, the chosen energy band must be much broader than the spectral width $\Delta\omega$. We have also checked convergence with the number of partial waves included in the close-coupling expansion of the electronic continuum states. We have found that the main contribution comes, as expected, from the lowest $l=1$ partial wave. Inclusion of additional partial waves implies doubling, tripling, and so on, the number of degenerate continuum states (hence the number of vibronic states). As in Ref. [18], we have included $l=1$ and 3 partial waves. Inclusion of more partial waves barely changes the results.

Convergence of the method by increasing the energy band ΔE (i.e., the number of states in the close-coupling equations) is illustrated in Fig. 2 for the $^1\Sigma_u^+$ symmetry in the photon energy range 25–28 eV and pulse duration $T=10$ fs. A continuum energy grid $\{\varepsilon_n'', n=1-150\}$ built with $\Delta k=0.01$ a.u. is used. This figure includes results for the vibrational distributions by successively increasing the energy band from $\Delta E=2-17$ eV. For instance, to show how the method works, in the case of photon energy $\omega=27$ eV, a

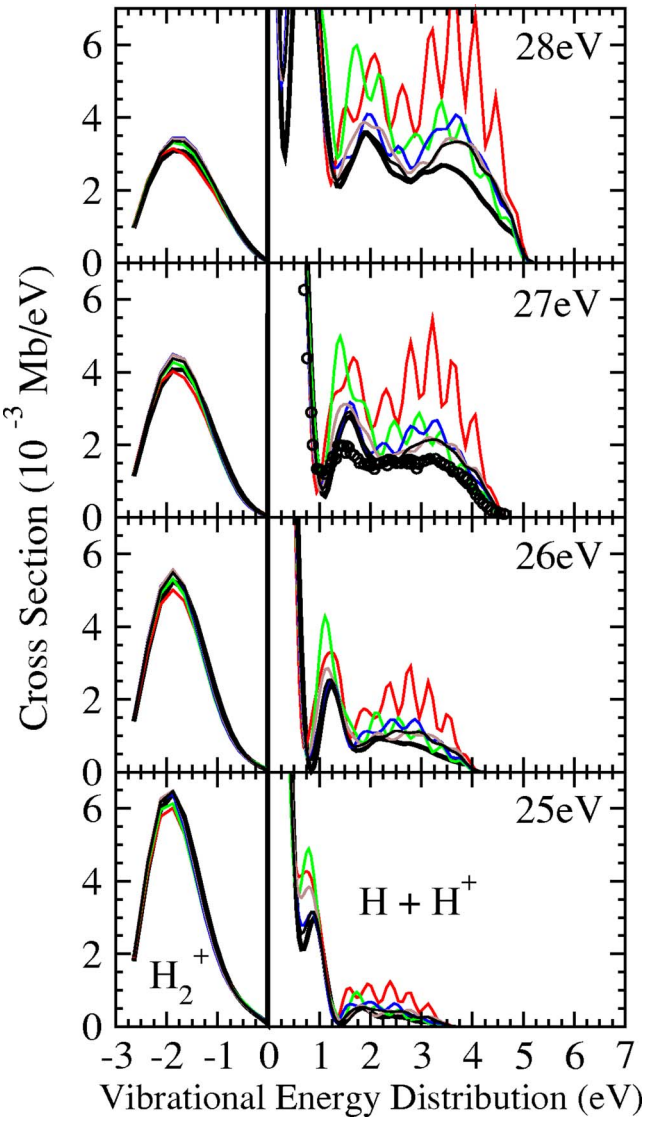

FIG. 2. (Color online) $^1\Sigma_u^+$ proton kinetic energy distribution (above 0 eV) in the photon energy range $\omega=25-28$ eV and a pulse duration of 10 fs. The vibrational distribution for H_2^+ formed in the nondissociative ionization process (below 0 eV) is also shown for completeness. Convergence of the results with the number of vibronic states (energy band, see text) is shown: $\Delta E=2$ (red), 4 (green), 8 (blue), 12 (brown), and 17 eV (thin black). Perturbative stationary result from Ref. [18], thick black line. Experimental results from Ref. [16], open circles.

selected band of $\Delta E=2$ eV results in nine vibrational states associated with the lowest Q_1 resonance (from $k_r=83$ to 91) and a varying number of vibrational states associated with an electronic continuum grid (ε_n'') $(n=1-95)$. In the latter case, the number of vibrational states ranges from 10 $(v_{H_2^+}=86-95)$ for the lowest electronic energy $\varepsilon_1''=\mathcal{E}(R)+0.005$ a.u. to 1 $(v_{H_2^+}=1)$ for the highest energy $\varepsilon_{95}''=\mathcal{E}(R)+0.451$ a.u.. This amounts to 2552 vibronic states to be included in the close-coupling equations. Convergence has been achieved for an energy band $\Delta E=17$ eV, which corresponds to 82 vibrational states associated with the lowest doubly excited state $(k_r=39-120)$ and a total of 21 748 vi-

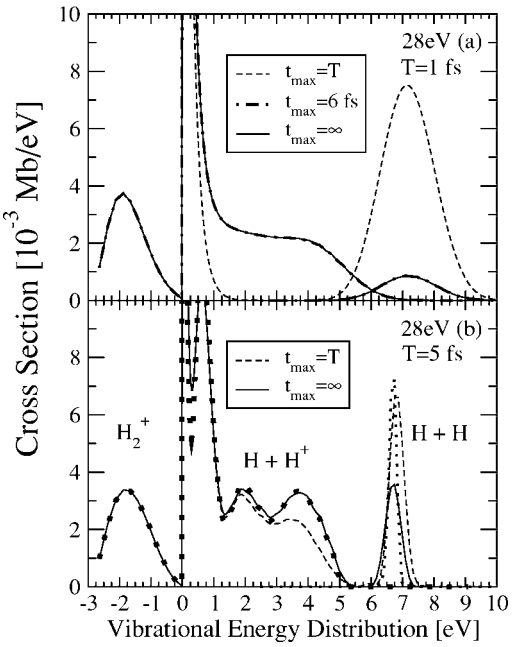

FIG. 3. $^1\Sigma_u^+$ proton kinetic energy distribution for dissociative photoionization (above 0 eV) and H kinetic energy distribution for the photodissociation of the Q_1 resonance (above 5 eV) at a photon energy $\omega=28$ eV and an energy band $\Delta E=17$ eV. The vibrational distribution for H_2^+ formed in the nondissociative ionization process (below 0 eV) is also shown for completeness. $T=1$ (a) and (b) 5 fs. Results from Fig. 2 for the pulse of $T=10$ fs are also included in (b) for comparison (dots).

bronic states associated with an electronic continuum grid (ε_n'') that goes from $n=1$ to 121. This energy band requires a memory allocation of 8 gigabytes. Figure 2 shows that the converged results are very close to the perturbative ones reported in [18], which are in excellent agreement with the experimental results of [16]. This is remarkable because the results are obtained with completely different approaches and we are using a relatively short pulse of 10 fs instead of a permanent radiation field.

To analyze the variation of the results with pulse duration, we have carried out calculations for pulses between 1 and 10 fs. A sample of our results for pulses of 1, 5, and 10 fs is shown in Fig. 3. We have chosen a photon energy of 28 eV because resonance effects in the KEDs shown in Fig. 2 are more important at this photon energy. These results have been obtained integrating the TDSE up to $t_{max} \gg T$ (i.e., $t_{max} \sim \infty$). For the sake of conciseness, all processes (dissociative and nondissociative ionization, as well as nonionizing dissociation) are shown simultaneously. It is clear from the figure that a pulse of at least 5 fs is required to resolve the resonant peaks that appear at proton kinetic energies of 1, 2, and 4 eV. For shorter pulses (e.g., 1 fs), a smooth KED is obtained. Nevertheless, the calculated spectrum still shows the outcome of autoionization. This is illustrated by calculations in which time integration is stopped at the end of the pulse, $t_{max}=T$ (see Fig. 3). For the 1 fs case, it can be seen that the vibrational distribution at the end of the pulse is just what one would expect for photon energies far from the resonance region: a Franck-Condon distribution of the final vibrational states with a rapid exponential decay of the KED at low proton kinetic energy. In addition, the H+H photodissociation process is substantially overestimated. The signature of autoionization, which always appears at higher proton energies [14], is only apparent when integration is extended up to 6 fs or more (i.e., when the system is allowed to decay after the pulse is gone). This extended time integration also leads to a substantial decrease of the H+H photodissociation probability. This means that the doubly excited state autoionizes in the absence of the radiation field due to the $\mathcal{P}\mathcal{H}_{el}\mathcal{Q}$ coupling and, consequently, interferences due to the presence of that field (and observed in the perturbative results) are not possible. Furthermore, the large bandwidth associated with the 1 fs pulse dilutes the details associated with specific vibrational states and removes sharp resonance structures. For the 5 fs pulse, the signature of autoionization is already apparent at the end of the pulse, but the system still decays at longer times. In this case, the presence of resonance peaks is very clear and the results are very similar to what is obtained with a pulse of 10 fs. Therefore, it can be concluded that, for a pulse of 10 fs, there is enough time to represent autoionization and that a further increase of the pulse length would not lead to significant variations. This conclusion (which is compatible with the fact that the autoionization lifetime of the lowest Q_1 $^1\Sigma_u^+$ doubly excited state in the Franck-Condon region is of the order of a few fs [27]) explains the good agreement between the TDSE and the perturbative results shown in Fig. 2.

Hence we can use the results obtained with a 10 fs pulse to visualize the onset of the different resonant structures in the perturbative regime. Figure 4 illustrates the time evolution of the vibrational distribution at a photon energy $\omega=28$ eV. The results at $t=200$ as, i.e., just at the beginning of the pulse, show the process of populating the Q_1 $^1\Sigma_u^+$ doubly excited state over a wide range of vibrational states (corresponding to hydrogen kinetic energies larger than 5 eV). This vibrational distribution narrows in time and its maximum is shifted down (due to the repulsive character of the potential energy curve associated to the doubly excited state). The first resonant peak in the proton KED is only apparent at $t=4$ fs around 1 eV. All the important features related with proton emission are already present at $t=6$ fs: the corresponding KED widens up to ~5 eV and exhibits three peaks. As discussed in [12], the low-energy peak corresponds to the interference between direct ionization and autoionization modulated by the nuclear motion. It is worth noting that the doubly excited state still decays after 6 fs, leading to a substantial enhancement of the higher-energy peak in the proton KED. The surviving vibrational population in the doubly excited state (the peak slightly below 7 eV) becomes nonautoionizing and contributes to the photodissociation into $H(1s)+H(nl)$ products. This latter process will be analyzed in detail later.

B. Dissociative photoionization in the photon energy range $\omega=30-37$ eV

In the 30–37 eV photon energy range, the Q_2 doubly excited states and the two electronic continua associated with

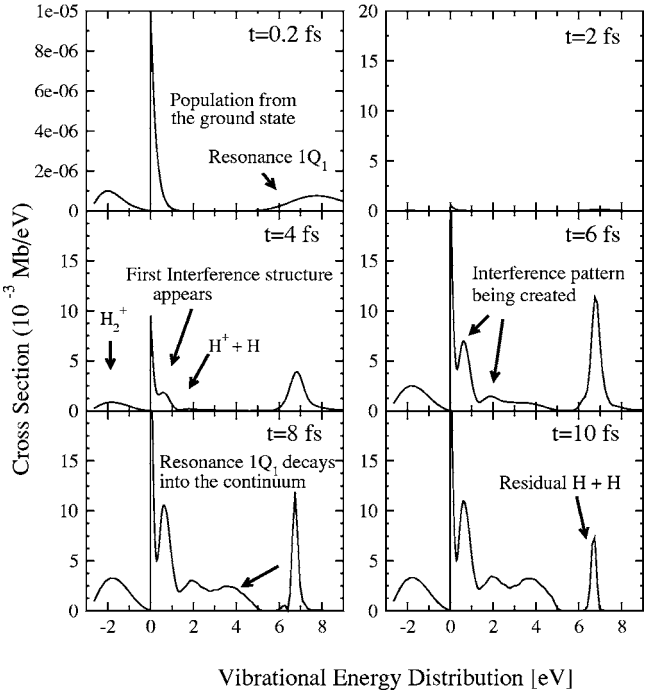

FIG. 4. Time evolution of $^1\Sigma_u^+$ proton kinetic energy distribution for dissociative photoionization (above 0 eV) and H kinetic energy distribution for the photodissociation of the Q_1 resonance (above 5 eV) at a photon energy $\omega=28$ eV, a pulse duration of 10 fs, and an energy band $\Delta E=17$ eV. The vibrational distribution for H_2^+ formed in the nondissociative ionization process (below 0 eV) is also shown for completeness. For the sake of clarity, at $t=0.2$ fs the y axis is scaled differently. For $t=2$ fs the shape is similar to that of $t=0.2$ fs but, due to the use of an extended scale, the corresponding curve can be barely seen.

the $^2\Sigma_g^+(1s\sigma_g)$ and $^2\Sigma_u^+(2p\sigma_u)$ ionization thresholds can be populated. All these channels must be included simultaneously in the calculations (see Fig. 1) and, consequently, the selected energy band ΔE must be even wider than in the previous section. To keep the size of the calculations to reasonable proportions, we have used a less dense electronic energy grid $\{\varepsilon_n'', n=1-150\}$ with $\Delta k=0.02$ a.u. This grid still satisfies the spectral width condition discussed in Sec. III C.

Figure 5 shows the proton KED in the final $^1\Sigma_u^+$ symmetry. In these series of computations, we have included the six lowest Q_1 and six lowest Q_2 $^1\Sigma_u^+$ doubly excited states. As explained in Sec. III A, the two electronic continua are computed using a different partitioning of the $\mathcal{P}$ and $\mathcal{Q}$ subspaces. All states enclosed in an energy band of $\Delta E=20$ eV have been included, which leads to 21 411 vibronic states for $\omega=30$ eV and up to 22 119 states for $\omega=37$ eV. We have used a pulse duration of $T=10$ fs. The calculated proton KEDs are in reasonable agreement with the most recent experimental results [17]. It can be seen that, as the photon energy increases, the fraction of protons with higher kinetic energy also increases. In fact, for $\omega=37$ eV, the proton KED is very well localized: very slow (~0 eV) or very fast (~8 eV) protons, and almost no resonant peaks in between. The two localized regions correspond to nonresonant ionization through the $^2\Sigma_g^+(1s\sigma_g)$ and $^2\Sigma_u^+(2p\sigma_u)$ ionization thresholds, respectively (see the corresponding partial cross sections in Fig. 5). The absence of resonance peaks at 37 eV (see Fig. 5) is due to the fact that the Q_1 doubly excited states lie outside the Franck-Condon region (see Fig. 1). Contribution of the Q_2 doubly excited states becomes relevant only above 37 eV. In the experiment, the peak arising at 4 eV for $\omega=37$ eV is due to the opening of the $^2\Pi_u(2p\pi_u)$ threshold, which is not included in our computations.

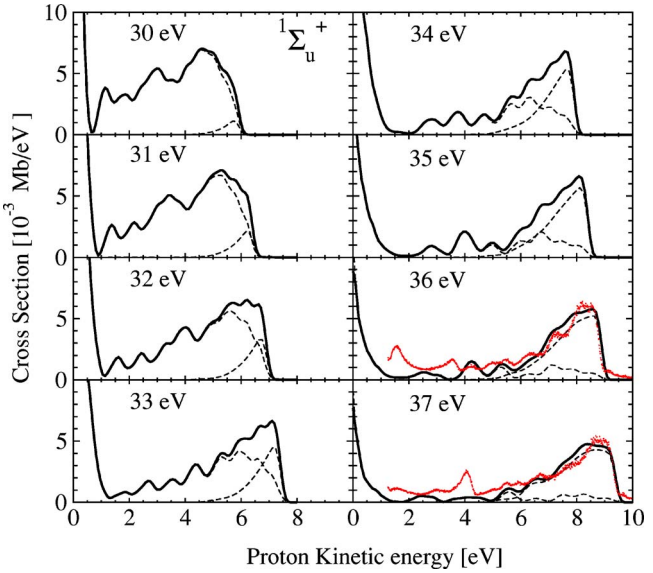

FIG. 5. (Color online) $^1\Sigma_u^+$ proton kinetic energy distribution of H_2 for protons detected at 0° in the photon energy range $\omega=30-37$ eV and a pulse duration of 10 fs. Dashed line at the lower kinetic energies, contribution from the $^2\Sigma_g^+(1s\sigma_g)$ ionization channel; dashed line at the higher kinetic energies, contribution from the $^2\Sigma_u^+(2p\sigma_u)$ ionization channel; thick solid line, sum; dots, experimental data from Ref. [17].

Similar calculations performed for the $^1\Pi_u$ symmetry are also in good agreement with the available experimental results from Refs. [16,17] and recent perturbative calculations [17].

C. Dissociation of doubly excited states into neutrals: H+H

One of the advantages of the present method is that it makes it possible to study photodissociation of doubly excited H_2 into neutral fragments. Although cross sections for the formation of $H(n=2)$ were determined for the first time in 1986 by Glass-Maujean [28,29] and Arai *et al.* [30,31] by measuring the Ly-α radiative emission of atomic hydrogen, a proper theoretical treatment that includes the competition between all possible ionization and dissociation channels is not yet available. As mentioned above, photodissociation from doubly excited states competes with autoionization for photon energies above ~23 eV. In our time-dependent method, the population that remains in the doubly excited states without being autoionized is directly related to this photodissociation process. As in the experiments of Refs. [28–31], here we will concentrate on the formation of $H(n=2)$.

In previous attempts to interpret the experimental results, Glass-Maujean [28,32,33] and Borges and Bielschowsky

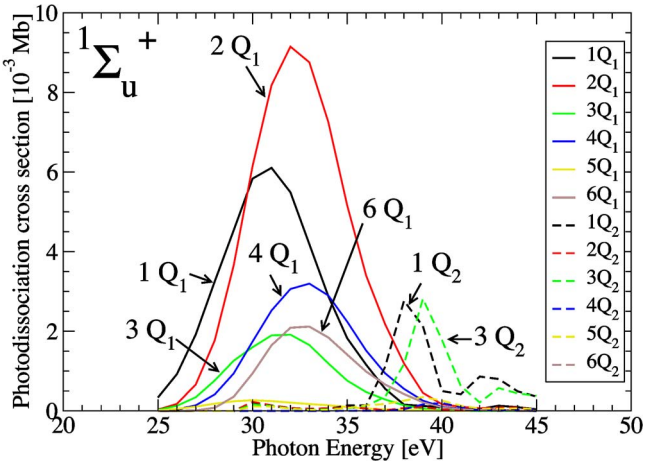

FIG. 6. (Color online) Photodissociation cross section into H+H via $^1\Sigma_u^+$ symmetry for the six lowest Q_1 and six lowest Q_2 resonances. The pulse duration is 10 fs.

[34,35] have made use of a simple empirical formula for the photodissociation cross section, $\sigma_d(E)=\chi_d\sigma_a(E)$, where $\sigma_a(E)$ is the absorption cross section from the ground state and χ_d is the dissociation yield or survival probability. The absorption cross section has been calculated within the Franck-Condon approximation [28,34]. The dissociation yield χ_d has been either estimated [28] or calculated semiclassically [34,35] assuming that it is independent of the photon energy. To obtain the corresponding photodissociation cross section from the TDSE, we have extended our computations up to a photon energy $\omega=45$ eV and integrated in H kinetic energy the calculated differential cross sections (a few examples of the latter are shown in Fig. 3). The pulse duration is 10 fs.

Figures 6 and 7 show the contributions of the six lowest Q_1 and six lowest Q_2 doubly excited states to the photodissociation cross section for the $^1\Sigma_u^+$ and $^1\Pi_u$ symmetries, respectively, in the photon energy range $\omega=25-45$ eV. In general, the contributions of individual doubly excited states do not follow a simple Franck-Condon behavior (e.g., sometimes the maxima are significantly shifted). Q_1 and Q_2 doubly excited states contributing to the formation of H(n=2) are (the dominant character is indicated within parentheses): $1Q_1$ $^1\Sigma_u^+(2p\sigma_u 2s\sigma_g)$, dissociating into H(1$s$)+H(2$s$); $2Q_1$ $^1\Sigma_u^+(2p\sigma_u 3d\sigma_g)$, dissociating into H(1$s$)+H(2$p$); $1Q_1$ $^1\Pi_u(2p\sigma_u 3d\pi_g)$, dissociating into H(1$s$)+H(2$p$); $1Q_2$ $^1\Sigma_u^+(2p\pi_u 3d\pi_g)$, contributing twice to H(2p), and the rest of nQ_2 $^1\Sigma_u^+$ ($n>1$), dissociating into H(2p)+H($n\geq 3$); $1Q_2$ $^1\Pi_u(2p\pi_u 2s\sigma_g)$, into H(2$p$)+H(2$s$), $2Q_2$ $^1\Pi_u(2p\pi_u 3d\sigma_g)$, twice to H(2$p$), and the rest of nQ_2 $^1\Pi_u$ ($n>2$), dissociating into H(2p)+H($n\geq 3$). The dominant configurations within parentheses correspond to the equilibrium internuclear distance. As in Ref. [27], the united and separate atom limits have been correlated following the well-known Barat-Lichten rules of molecular orbitals [36].

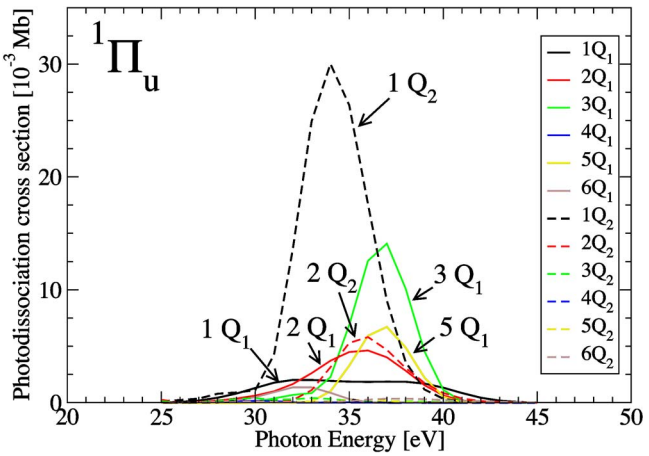

FIG. 7. (Color online) Photodissociation cross section into H+H via $^1\Pi_u$ symmetry for the six lowest Q_1 and six lowest Q_2 resonances. The pulse duration is 10 fs.

The Q_1 $^1\Sigma_u^+$ and $^1\Pi_u$ doubly excited states cross the $^2\Sigma_g^+(1s\sigma_g)$ ionization threshold at $R\geq 4$ a.u. (see Fig. 1), then they become nonautoionizing and exhibit avoided crossings with an infinite number of H_2 Rydberg states of the same symmetry lying below the threshold. In practice, this infinite series of Rydberg states is excluded from the $\mathcal{Q}$ subspace due to the partitioning used in the Feshbach formalism. In principle, a correct description of the dissociation dynamics should take into account these avoiding crossings, but, as treating an infinite number of avoided crossings is complicated in practice, we have assumed a complete diabatic behavior of the Q_1 doubly excited states so that the corresponding repulsive energy curves are smoothly correlated to the asymptotic limits of the six lowest singly excited states of H_2 [37,38]. In contrast with the Q_1 states, there is no problem with the Q_2 doubly excited states, since they do not cross any ionization threshold and they dissociate directly into excited states of the atomic hydrogen.

Figure 8 shows a comparison of the calculated H(n=2) cross section with the experimental results of Ref. [29], extracted from the Ly-α emitted radiation. The experimental cross sections have been renormalized to our theoretical result. The H(n=2) cross section has also been measured by Arai *et al.* [30], but since their results (in arbitrary units) are practically identical to those of Glass-Maujean, they have not been included in the figure. The calculated cross section is roughly a factor of three larger than the experimental ones. However, one must take into account that what is measured is the Lyman-α radiative cross section while what is calculated in the present work is the cross section for H(n=2) production, which must be an upper bound to the former. In this respect it is worth noticing that the absolute value of the calculated photoionization cross section is in excellent agreement with the experimental values of Latimer *et al.* [39] and with the perturbative calculations of Sánchez and Martín [19]. Therefore, one should expect a similar accuracy in the calculated photodissociation cross section.

The overall shape of the calculated and measured cross sections is very similar for photon energies smaller than 36 eV. In particular, the shoulder observed in the experiments at around 28 eV is well reproduced by the theory. Above 36 eV, the calculated cross section decreases rapidly, while the experimental one remains more or less constant. The reason for this discrepancy is the opening of the

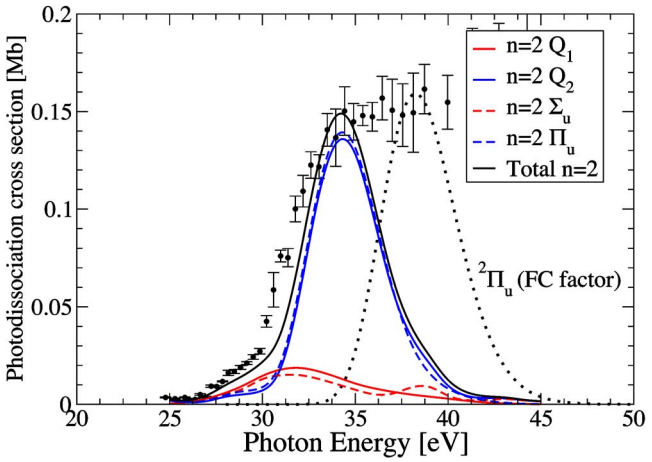

FIG. 8. (Color online) Cross section for H(n=2) production via photodissociation of autoionizing states of H_2. Contributions from Q_1 and Q_2 ($^1\Sigma_u^+$ plus $^1\Pi_u$) doubly excited states and from $^1\Sigma_u^+$ and $^1\Pi_u$ symmetries (Q_1 plus Q_2) are shown. The total H(n=2) production is compared with experimental results of Ref. [29]. Scaled Franck-Condon factors for the transition $X\,^1\Sigma_g^+(H_2)\rightarrow{}^2\Pi_u(H_2^+)+e^-$ is also included (see text). The pulse duration used in the calculations is 10 fs.

$^2\Pi_u(2p\pi_u)$ ionization channel (not included in the present calculations), which leads to dissociation into H^++H($2p$) and thus contributes to the measured Ly-α emission. This is illustrated in Fig. 8 by the Franck-Condon factor associated with the $X\,^1\Sigma_g^+(H_2)\rightarrow{}^2\Pi_u(H_2^+)+e^-$ transition. This factor takes a maximum value around 38 eV. Therefore, Ly-α emission above 36 eV results from dissociative ionization into H($2p$)+H^++e^- and not from photodissociation of H_2 doubly excited states leading to H(n=2). The figure also shows that contributions from the Q_1 states are practically restricted to the lower-energy region and to the $^1\Sigma_u^+$ symmetry, while contributions from the Q_2 states are largely dominant above 32 eV and almost entirely due to states of $^1\Pi_u$ symmetry. Thus any possible inaccuracy due to our diabatization of the Q_1 states below the ionization threshold has no practical implication in the calculated H(n=2) cross section above 32 eV. Among the Q_2 states, the most important contribution comes from the $1Q_2\,^1\Pi_u$ state (see Fig. 7). This state contributes twice to the H(n=2) emission. Within the $Q_1\,^1\Sigma_u^+$ manifold, the first and the second states are the most significant ones (see Fig. 6). These results are at variance with the analysis performed by Glass-Maujean [28,33], who has concluded that the $1Q_1$ Π_u and $1Q_2$ Π_u doubly excited states are the dominant ones. Our results are also different from those obtained in Ref. [34] with a semiclassical method. In this respect, it is worth pointing out that such a discrepancy appears even though the autoionization widths used by Borges and Bielschowsky [34] are identical to those obtained in the present work from the $\mathcal{PHQ}$ matrix elements.[1] In fact, they find much better agreement with experiment by using less accurate values of these widths. This comparison shows that the use of semiclassical methods in the present context, where interferences modulated by the nuclear motion significantly affect autoionization, can be dangerous in interpreting the experimental observations. A similar failure of the semiclassical approximation in electron impact ionization of H_2 has been reported [40].

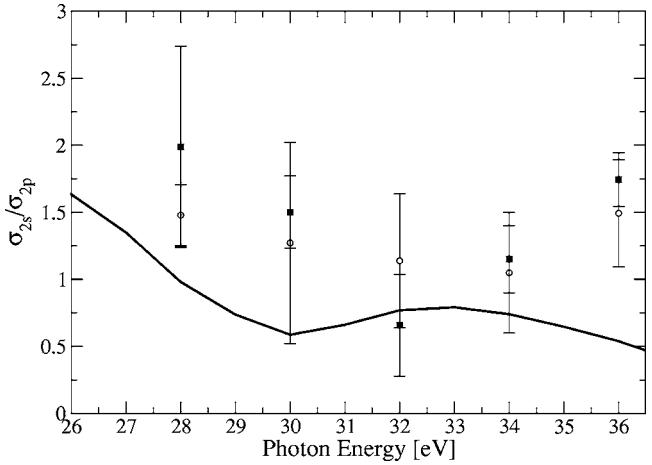

FIG. 9. $\sigma(2s)/\sigma(2p)$ ratio for H+H photodissociation. Experimental results from Refs. [32,33]. The pulse duration used in the calculations is 10 fs.

Very recently, Glass-Maujean and co-workers [32,33] have reexamined the dissociation dynamics of doubly excited states of H_2 by providing the $\sigma(2s)/\sigma(2p)$ ratio for a reduced number of photon energies. Within the large experimental error bars, the measured ratio is close to one for all photon energies with smooth oscillations around this value [32,33]. This finding is compatible with our theoretical results shown in Fig. 9 in the photon energy range in which the theoretical calculations are meaningful.

Arai *et al.* [31] have also performed measurements of photodissociation producing H($2p$)+H($2p$) atoms by detecting two Ly-α photons in coincidence. In our scheme, dissociation into H($2p$)+H($2p$) can only proceed through two different doubly excited states: the $1Q_2\,^1\Sigma_u^+(2p\pi_u 3d\pi_g)$ state and the $2Q_2\,^1\Pi_u(2p\pi_u 3d\sigma_g)$ one. Therefore, the corresponding cross section is only a small fraction of the total photodissociation cross section. In Fig. 10 we compare the calculated H($2p$)+H($2p$) cross section with the experimental one [31], which has been renormalized at the maximum. The agreement is good. The dominant contribution comes from the $2Q_2\,^1\Pi_u$ state, except at the rising edge between 29 and 32 eV. Again, our results are much closer to the experimental observations than those obtained by using semiclassical methods [34,35].

V. CONCLUSION

A nonperturbative time-dependent method has been developed to describe autoionization of H_2 doubly excited states and its manifestation in dissociative and nondissociative ionization when the molecule interacts with xuv fs laser

[1] Although the present theoretical approach does not make explicit use of autoionization widths, the latter can be easily obtained from the calculated wave functions; the corresponding widths are identical to those reported in Ref. [27].

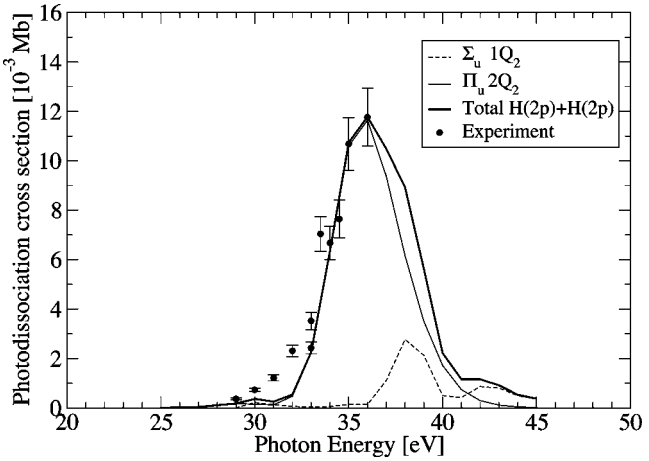

FIG. 10. Photodissociation cross section of H_2 into $H(2p)+H(2p)$ via the first Q_2 $^1\Sigma_u^+$ and the second Q_2 $^1\Pi_u$ doubly excited states. Experimental results from Ref. [31]. The pulse duration used in the calculations is 10 fs.

pulses. The method includes all electronic and vibrational degrees of freedom and can therefore describe competition and interferences between all open ionization and/or dissociation channels. The method has been tested by comparing with the kinetic energy distribution obtained by using stationary perturbation theory in the region where Q_1 and Q_2 doubly excited states are populated. Good agreement with the perturbative results and with experiment has been found for pulse durations of 10 fs or more and an intensity of 10^{12} W/cm^2.

By varying the pulse duration, we have analyzed variations in the autoionization patterns. In particular, for 1 fs pulses, sharp resonant structures disappear but autoionization is still visible if one waits long enough after the pulse is gone. This is very attractive because it suggests that pump-probe experiments, in which the pump is a 1 fs xuv pulse and the probe is a longer ir pulse, can be used to observe the time evolution of autoionization decay in simple molecules and to analyze in great detail how the nuclear motion affects this decay.

We have also provided a realistic theoretical study of H_2 photodissociation mediated by doubly excited states. This process occurs when the doubly excited states do not autoionize and the molecule follows the corresponding repulsive potential energy curve that leads to two hydrogen atoms. Contributions to this process from the six lowest doubly excited states of both Q_1 and Q_2 series and both $^1\Sigma_u^+$ and $^1\Pi_u$ symmetries have been reported. The calculated cross sections for the production of $H(n=2)$ and $H(2p)+H(2p)$ are in good agreement with experimental results obtained by measuring the emitted Ly-α radiation.

Although conceptually simple and fast, the method demands a large computer memory allocation. The advent of supercomputers with large global shared memory solve this problem effectively. Therefore, it can be expected that such a method can be used in the near future to treat more sophisticated problems such as multiphoton ionization involving molecular doubly excited states or the behavior of the latter states in the presence of strong nonperturbative laser fields.

ACKNOWLEDGMENTS

This work was supported by the DGI (Spain) Project No. BFM2003-00194 and the European COST Action No. D26/0002/02. J.L.S.-V. acknowledges a Comisión de Servicios granted by the Universidad de Antioquia and funding by CIEN (UdeA) and Colciencias agency (Colombia). He also acknowledges financial support from the Spanish Ministerio de Educación y Ciencia under Project No. BFM2003-00194. We also thank Professor Michele Glass-Maujean and Professor Kenji Ito for providing us the experimental data files and clarifying comments.

[1] J. Andruszkow *et al.*, Phys. Rev. Lett. **85**, 3825 (2000).
[2] H. Wabnitz *et al.*, Nature (London) **420**, 482 (2002).
[3] V. Ayvazyan *et al.*, Phys. Rev. Lett. **88**, 104802 (2002).
[4] P. Agostini and L. F. DiMauro, Rep. Prog. Phys. **67**, 813 (2004).
[5] R. Klenberger *et al.*, Nature (London) **427**, 817 (2004).
[6] H. Mashiko, A. Suda, and K. Midorikawa, Opt. Lett. **29**, 1927 (2004).
[7] T. Laarmann, A. R. B. deCastro, P. Gürtler, W. Laasch, J. Schulz, H. Wabnitz, and T. Möller, Phys. Rev. A **72**, 023409 (2005).
[8] J. H. Posthumus, Rep. Prog. Phys. **67**, 623 (2004).
[9] N. Miyamoto, M. Kamei, D. Yoshitomi, T. Kanai, T. Sekikawa, T. Nakajima, and S. Watanabe, Phys. Rev. Lett. **93**, 083903 (2004).
[10] Y. Nabekawa, H. Hasegawa, E. J. Takahashi, and K. Midorikawa, Phys. Rev. Lett. **94**, 043001 (2005).
[11] M. Drescher, M. Hentschel, R. Kienberger, M. Uiberacker, V. Yakovlev, A. Scrinzi, T. Westerwalbesloh, U. Kleineberg, U. Heinzmann, and F. Krausz, Nature (London) **419**, 803 (2002).
[12] I. Sánchez and F. Martín, Phys. Rev. Lett. **79**, 1654 (1997).
[13] I. Sánchez and F. Martín, Phys. Rev. Lett. **82**, 3775 (1999).
[14] S. Strathdee and R. Browning, J. Phys. B **12**, 1789 (1979).
[15] C. J. Latimer, J. Geddes, M. A. MacDonald, N. Kouchi, and K. F. Dunn, J. Phys. B **29**, 6113 (1996).
[16] K. Ito, R. I. Hall, and M. Ukai, J. Chem. Phys. **104**, 8449 (1996).
[17] T. Aoto, Y. Hikosaka, R. I. Hall, K. Ito, J. Fernández, and F. Martín, Chem. Phys. Lett. **389**, 145 (2004).
[18] I. Sánchez and F. Martín, Phys. Rev. A **57**, 1006 (1998).
[19] I. Sánchez and F. Martín, J. Chem. Phys. **107**, 8391 (1997).
[20] S. Barmaki, H. Bachau, and M. Ghalim, Phys. Rev. A **69**, 043403 (2004).
[21] A. Palacios, H. Bachau, and F. Martín, J. Phys. B **38**, L99 (2005).
[22] A. Palacios, S. Barmaki, H. Bachau, and F. Martín, Phys. Rev. A **71**, 063405 (2005).

[23] A. Palacios, H. Bachau, and F. Martín, Phys. Rev. Lett. (to be published).
[24] I. Sánchez and F. Martín, J. Phys. B **30**, 679 (1997).
[25] F. Martín, J. Phys. B **32**, R197 (1999).
[26] F. Martín, Phys. Rev. A **48**, 331 (1993).
[27] I. Sánchez and F. Martín, J. Chem. Phys. **106**, 7720 (1997).
[28] M. Glass-Maujean, J. Chem. Phys. **85**, 4830 (1986).
[29] M. Glass-Maujean, J. Chem. Phys. **89**, 2839 (1988).
[30] S. Arai, T. Yoshimi, M. Morita, K. Hironaka, T. Yoshida, H. Koizumi, K. Shinsaka, Y. Hatano, A. Yagishita, and K. Ito, Z. Phys. D: At., Mol. Clusters **4**, 65 (1986).
[31] S. Arai, T. Kamosaki, M. Ukai, K. Shinsaka, Y. Hatano, Y. Ito, H. Koizumi, A. Yagishita, K. Ito, and K. Tanaka, J. Chem. Phys. **88**, 3016 (1988).
[32] M. Glass-Maujean, S. Klumpp, L. Werner, A. Ehresmann, and H. Schmoranzer, J. Phys. B **37**, 2677 (2004).
[33] M. Glass-Maujean and H. Schmoranzer, J. Phys. B **38**, 1093 (2005).
[34] I. Borges, Jr., and C. E. Bielschowsky, J. Phys. B **33**, 1713 (2000).
[35] I. Borges, Jr., and C. E. Bielschowsky, Chem. Phys. Lett. **342**, 411 (2001).
[36] M. Barat and W. Lichten, Phys. Rev. A **6**, 211 (1972).
[37] G. Staszewska and L. Wolniewicz, J. Mol. Spectrosc. **212**, 208 (2002).
[38] L. Wolniewicz and G. Staszewska, J. Mol. Spectrosc. **217**, 181 (2003).
[39] C. J. Latimer, K. F. Dunn, F. P. O'Neill, M. A. MacDonald, and N. Kouchi, J. Chem. Phys. **102**, 722 (1995).
[40] F. Martín, J. Phys. B **32**, L181 (1999).